

AFWAL-TR-87-4011

ADA181243



RESEARCH ON MECHANICAL PROPERTIES
FOR ENGINE LIFE PREDICTION

N. E. ASHBAUGH
M. KHOBAIB
G. A. HARTMAN
T. WEERASOORIYA
D. C. MAXWELL
R. C. GOODMAN

UNIVERSITY OF DAYTON
RESEARCH INSTITUTE
DAYTON, OHIO 45469

MAY 1987

INTERIM REPORT FOR PERIOD COVERING
1 AUGUST 1985 THROUGH 31 JULY 1986

APPROVED FOR PUBLIC RELEASE; DISTRIBUTION UNLIMITED

MATERIALS LABORATORY
AIR FORCE SYSTEMS COMMAND
AIR FORCE WRIGHT AERONAUTICAL LABORATORIES
WRIGHT-PATTERSON AIR FORCE BASE, OHIO 45433-6533

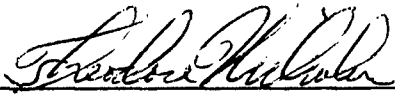
20040224225

NOTICE

When Government drawings, specifications, or other data are used for any purpose other than in connection with a definitely related Government procurement operation, the United States Government thereby incurs no responsibility nor any obligation whatsoever; and the fact that the government may have formulated, furnished, or in any way supplied the said drawings, specifications, or other data, is not to be regarded by implication or otherwise as in any manner licensing the holder or any other person or corporation, or conveying any rights or permission to manufacture use, or sell any patented invention that may in any way be related thereto.

This report has been reviewed by the Office of Public Affairs (ASD/PA) and is releasable to the National Technical Information Service (NTIS). At NTIS, it will be available to the general public, including foreign nations.

This technical report has been reviewed and is approved for publication.

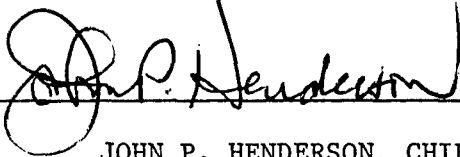


THEODORE NICHOLAS
METALS BEHAVIOR BRANCH
METALS AND CERAMICS DIVISION



ALLAN W. GUNDERSON
TECH AREA MANAGER
METALS BEHAVIOR BRANCH
METALS AND CERAMICS DIVISION

FOR THE COMMANDER



JOHN P. HENDERSON, CHIEF
METALS BEHAVIOR BRANCH
METALS AND CERAMICS DIVISION

If your address has changed, if you wish to be removed from our mailing list, or if the addressee is no longer employed by your organization please notify AFWAL/MLLN, W-PAFB, OH 45433 to help us maintain a current mailing list.

Copies of this report should not be returned unless return is required by security considerations, contractual obligations, or notice on a specific document.

REPORT DOCUMENTATION PAGE

1a. REPORT SECURITY CLASSIFICATION Unclassified		1b. RESTRICTIVE MARKINGS	
2a. SECURITY CLASSIFICATION AUTHORITY		3. DISTRIBUTION/AVAILABILITY OF REPORT Approved for public release; distribution unlimited.	
2b. DECLASSIFICATION/DOWNGRADING SCHEDULE			
4. PERFORMING ORGANIZATION REPORT NUMBER(S) UDR-TR-86-141		5. MONITORING ORGANIZATION REPORT NUMBER(S) AFWAL-TR-87-4011	
6a. NAME OF PERFORMING ORGANIZATION University of Dayton Research Institute	6b. OFFICE SYMBOL (If applicable)	7a. NAME OF MONITORING ORGANIZATION Materials Laboratory (AFWAL/MLLN) Air Force Wright Aeronautical Laboratories	
6c. ADDRESS (City, State and ZIP Code) 300 College Park Drive Dayton, Ohio 45469		7b. ADDRESS (City, State and ZIP Code) Wright-Patterson AFB, Ohio 45433-6533	
8a. NAME OF FUNDING/SPONSORING ORGANIZATION	8b. OFFICE SYMBOL (If applicable)	9. PROCUREMENT INSTRUMENT IDENTIFICATION NUMBER F33615-84-C-5051	
8c. ADDRESS (City, State and ZIP Code)		10. SOURCE OF FUNDING NOS.	
		PROGRAM ELEMENT NO. 61102F	PROJECT NO. 2302
		TASK NO. P1	WORK UNIT NO. 18
11. TITLE (Include Security Classification) Research on Mechanical Properties for Engine Life Prediction			
12. PERSONAL AUTHOR(S) N.E. Ashbaugh, M. Khobaib, G.A. Hartman, T. Weerasooriya, D.C. Maxwell, R.C. Goodman			
13a. TYPE OF REPORT Interim	13b. TIME COVERED FROM 8/1/85 TO 7/31/86	14. DATE OF REPORT (Yr., Mo., Day) May 1987	15. PAGE COUNT 70
16. SUPPLEMENTARY NOTATION			
17. COSATI CODES		18. SUBJECT TERMS (Continue on reverse if necessary and identify by block number)	
FIELD	GROUP	SUB. GR.	Laser interferometer system, compliance, fatigue crack closure, surface crack, fatigue crack growth, (over)
11	06		
01	03		
19. ABSTRACT (Continue on reverse if necessary and identify by block number)			
<p>Analytical and experimental investigations have been performed to determine crack growth behavior of turbine engine disk and blade alloys under various loading conditions typical of service environments. Tests were performed at elevated temperature in vacuum also to evaluate the baseline crack growth behavior. Substructural analysis of creep rupture specimens were conducted to understand the basic mechanism of time-dependent elevated temperature deformation. The work performed can be divided into three categories -- development of experimental techniques, material characterization techniques, and data maintenance and test support activities.</p> <p>The capability of the IDG laser system to monitor extended gage length was analyzed and found feasible. New grips and specimens have been designed and fabricated for high temperature composite testing. Enhancements to existing systems for crack length and displacement measurements were made. A number of computer automation applications are also discussed. (over)</p>			
20. DISTRIBUTION/AVAILABILITY OF ABSTRACT UNCLASSIFIED/UNLIMITED <input checked="" type="checkbox"/> SAME AS RPT. <input type="checkbox"/> DTIC USERS <input type="checkbox"/>		21. ABSTRACT SECURITY CLASSIFICATION Unclassified	
22a. NAME OF RESPONSIBLE INDIVIDUAL Theodore Nicholas		22b. TELEPHONE NUMBER (Include Area Code) 513-255-2689	22c. OFFICE SYMBOL AFWAL/MLLN

BLOCK 18 (Concluded)

environmental interaction, notches, creep crack growth, creep rupture, stacking faults, hot corrosion, test automation, nickel-based superalloys, ceramic composites, single crystal material.

BLOCK 19 (Concluded)

Fatigue crack closure, fatigue and creep crack growth, and creep rupture and hot corrosion tests were conducted. Descriptions of the experimental techniques and results of these tests are described.

FOREWORD

The work described in this report was performed at the Metals Behavior Branch, Metals and Ceramics Division, Materials Laboratory, Air Force Wright Aeronautical Laboratories (AFWAL/MLLN) under Contract No. F33615-84-C-5051, "Research on Mechanical Properties for Engine Life Prediction." The contract is administered under the direction of AFWAL by Dr. Theodore Nicholas (MLLN). The program is being conducted by the Structural Integrity Division, University of Dayton Research Institute, Dayton, Ohio with Dr. Noel E. Ashbaugh as the Principal Investigator. This report is the second annual report on the progress on the three-year contract.

The investigations were conducted by Drs. Noel E. Ashbaugh, M. Khobaib, Tusit Weerasooriya, and Messer George Hartman, III. Generation of the data was accomplished in part by Messers. Richard Goodman, David Maxwell, George Ahrens, David Johnson, William Goddard, and Mrs. Susan Ramsey. Assistance in data reduction, computer programming, fabrication of fixtures, and assembling mechanical and electrical components has been provided by Messers. Joe Cook, Paul Enderle, and Todd North and Miss Pat Bornhorst. Miss Debbie Garner was responsible for the typing of this document. This work was performed during the period 1 August 1985 to 31 July 1986.

TABLE OF CONTENTS

<u>SECTION</u>		<u>PAGE</u>
1	INTRODUCTION	1
2	EXPERIMENTAL DEVELOPMENT	3
	2.1 MEASUREMENT TECHNIQUES	3
	2.1.1 <u>Extended Gage Length for the IDG Laser System</u>	3
	2.1.2 <u>Ceramic Composite Testing</u>	4
	2.1.3 <u>Crack Length Expression as a Function of Compliance for Center Cracked Tension Specimens</u>	6
	2.2 TEST SYSTEM AUTOMATION	8
	2.2.1 <u>Software Enhancements on IBM System 9000</u>	9
	2.2.2 <u>Improvements to the C20 HCF/LCF System</u>	10
	2.2.3 <u>Software Enhancements for PC Test Control System</u>	10
	2.3 REPAIR AND IMPROVEMENT OF THE INSTRON MAJOR/MINOR SYSTEM	12
3	MATERIAL CHARACTERIZATION	15
	3.1 CRACK CLOSURE	15
	3.1.1 <u>Effects of Load History and Specimen Geometry on Fatigue Crack Closure Measurements</u>	15
	3.1.2 <u>Effect of Closure on the Crack Growth of Surface Cracks in a High Strength Titanium Alloy</u>	16

TABLE OF CONTENTS (Continued)

<u>SECTION</u>	<u>PAGE</u>
3.2	FATIGUE CRACK GROWTH BEHAVIOR OF IN718 17
3.2.1	<u>Fatigue Crack Growth at High Load Ratios in the Time-Dependent Regime</u> 17
3.2.2	<u>Environmental Interaction as a Function of Frequency for Inconel 718</u> 18
3.2.3	<u>Crack Growth From Notches</u> 19
3.3	CRACK GROWTH BEHAVIOR OF SINGLE CRYSTALLINE MATERIAL 21
3.3.1	<u>Fatigue Crack Growth in Alloy N4</u> 23
3.3.2	<u>Fatigue Crack Growth of Alloy N4 in Vacuum</u> 23
3.3.3	<u>Creep Crack Growth of Alloy N4 in Laboratory Air</u> 24
3.3.4	<u>Creep Crack Growth of Alloy N4 in Vacuum</u> 24
3.3.5	<u>Fracture Surface Analysis of Creep Crack Growth Specimens</u> 26
3.3.6	<u>Creep Crack Growth of IN718</u> 26
3.4	MICROSTRUCTURE EVALUATIONS OF CREEP RUPTURE IN SINGLE CRYSTALLINE MATERIAL 29
3.4.1	<u>Creep Rupture Tests of Alloy N4</u> 29
3.4.2	<u>Substructural Analysis of Creep Tested Specimen at 1600°F</u> 31
3.4.3	<u>Development of Substructure at 1400°F, 1600°F, 1800°F, and 2000°F</u> 40

TABLE OF CONTENTS (Concluded)

<u>SECTION</u>		<u>PAGE</u>
	3.4.4 <u>Analysis of Stacking Faults</u>	44
3.5	FATIGUE LOADING AT HIGH FREQUENCY	52
	3.5.1 <u>High Frequency Fatigue</u> <u>Evaluation of Nickel-Base</u> <u>Sheet Material</u>	52
	3.6 HOT CORROSION TESTS	52
4	DATA MAINTENANCE AND TEST SUPPORT ACTIVITIES	54
	4.1 DATA TRANSMISSION AND STORAGE	
	4.2 MLLS BRANCH TEST SUPPORT ACTIVITIES	54
5	SUMMARY	56
REFERENCES		59

LIST OF ILLUSTRATIONS

<u>FIGURE</u>		<u>PAGE</u>
1	Center-Cracked Tension Specimen-M(T).	7
2	Periodic Single Overload Spectrum.	11
3	da/dN vs. Crack Length Behavior of Crack Growing From a Notch.	22
4	Crack Layering.	25
5	Crack Growth Behavior of Specimen with $\langle 101 \rangle / \langle 010 \rangle$ Orientation Tested at 1600°F in Vacuum.	27
6	Crack Growth Behavior of Specimen with $\langle 001 \rangle / \langle 010 \rangle$ Orientation Tested at 1600°F in Vacuum.	28
7	da/dt vs. K_{max} for 0.4-Inch-Thick IN718 Specimen Tested at 1200°F in Vacuum.	30
8	TEM Microstructure of Heat-Treated, Rene' N4 Single Crystal.	32
9	Substructure Developed at 0.15% Creep Strain.	33
10	Substructure Developed at 0.85% Creep Strain Tested at 1600°F.	34
11	Substructure Developed at 2.5% Creep Strain Tested at 1600°F.	37
12	Substructure Developed at >10.0% Creep Strain Tested at 1600°F.	39
13	Substructure Developed in the Creep Ruptured Specimen at 1400°F.	41
14	Substructure Developed in Creep-Ruptured Specimen at 1600°F.	42
15	Substructure Developed in Creep-Ruptured Specimen at 1800°F.	43
16	Substructure Developed in Creep-Ruptured Specimen at 2000°F.	46
17	Different Sets of Stacking Faults Developed at 1600°F.	49

SECTION 1

INTRODUCTION

This program emphasizes the experimental determination of the advanced mechanical properties, primarily the characterization of crack growth behavior of typical turbine engine disk and blade alloys under a broad range of conditions representative of those encountered in service. The information, obtained under this program, is of a form which can be utilized in life prediction methodologies which are based on the concept of damage tolerance as a design philosophy. The experimental investigations and the support of analytical modeling address materials and environments typical of those encountered in service and concentrate on those areas where current life prediction schemes are weakest or totally lacking. The emphasis is to provide experimental data and to model the fundamental aspects of fatigue in engine alloys. Innovative ideas are used in the investigations and resolution of existing and anticipated material behavior problems in aircraft turbine engines.

The research effort for the reporting period is subdivided into three interrelated research tasks:

- Experimental Development
- Material Characterization
- Data Maintenance and Test Support Activities

These tasks form an umbrella that covers many investigations which support major advances in the development of models for life prediction of engine related cracking problems. The following sections discuss work in progress and work completed under the individual tasks.

SECTION 2

EXPERIMENTAL DEVELOPMENT

2.1 MEASUREMENT TECHNIQUES

In the past year, several measurement techniques were evaluated and developed. A successful feasibility study was conducted to extend the capability of the IDG laser system to measure gage length from 0.1 mm to approximately 10 mm. In the area of composite testing, an extensive literature search and evaluation of gripping methods led to the development of a flat plate friction grip and proper specimen design for composite testing. In the on-going pursuit of crack growth related research for improved life prediction methodology, a simple expression was developed to express the crack length as a function of compliance for center-cracked tension specimens.

2.1.1 Extended Gage Length for the IDG Laser System

The short gage length (0.1 mm) of the laser interferometer system is ideal for studying crack tip response and other small-scale localized phenomena. Additional applications for non-contact displacement measurement methods, however, require a longer gage length on the order of 10 mm. To accommodate these needs, a task was established to evaluate methods of extending the gage length in stages from the current 0.1 mm to approximately 10.0 mm. The initial evaluations were successful on the optics bench and indicate that special optics and data reduction algorithms need to be developed.

2.1.2 Ceramic Composite Testing

With the increasing drive to operate jet turbine engines at higher temperatures and efficiencies, there is a great deal of interest in evaluating materials with extended temperature range capabilities. The ceramics and ceramic composite materials are promising candidates for engine applications since a number of them retain strength at temperatures exceeding 2000°F. Two of the drawbacks of these materials are their low ductility and the difficulty in manufacturing or fabrication. For laboratory tests, the low ductility produces high notch sensitivity and causes joining/gripping problems. The current high manufacturing cost means that large samples are not available or are prohibitively expensive. Due to these problems, standard laboratory test techniques cannot be used to produce meaningful test data to evaluate the behavior of ceramic and ceramic composite materials.

A task was initiated to develop test techniques and equipment which can be used to study the behavior of ceramic composite materials under elevated temperature and nonisothermal conditions. Following are the three main interrelated areas of prime concern in developing the test capability.

1. Sample Gripping - The brittle and anisotropic nature of ceramic composites makes it difficult to design specimens and gripping fixtures which will produce a uniform stress field in the test specimen section. The use of both cool grips where the grips are not in the furnace hot zone and hot grips are being considered.

2. Displacement Measurement - Because of their low ductility, ceramic composites are sensitive to stress discontinuities. Mechanical extensometers typically require attachments or introduce marks on the surface of the sample at the contact points which can produce premature failure. Specimen access for extensometry and small gage length must also be considered.

3. Sample Heating - Some of the proposed ceramic composite materials have usable strength at temperatures exceeding 3000°F. A number of heating techniques are available to attain this high temperature; however, very few can be adapted for use in the material-testing context. Specimen access for extensometry and gripping problems further augment the limitations.

Preliminary evaluations of gripping methods have led to the development of a flat-plate friction grip and specimen design which appear to meet the testing requirements. Approximately 12 tests have been performed at room temperature on a carbon-carbon composite with good results. High temperature versions of the grips are currently being designed and specimens of a barium magnesium aluminum silicate (BMAS) matrix composite are being fabricated.

Initially, conventional high-temperature extensometry will be used to measure displacement. As the temperature capability of the test system is increased, we plan to utilize a laser interferometric technique to provide displacement measurement capability at temperatures beyond the current mechanical extensometry limits.

A heating system using infrared quartz lamps is being assembled for use in the tests. In this design, since the lamp output is highly directional, the heating energy can be directed at the specimen test section only; this allows the grips to be maintained at a lower temperature. The proposed system will have provisions for access to the specimen for extensometry.

2.1.3 Crack Length Expression as a Function of Compliance for Center Cracked Tension Specimens

The object of this investigation was to formulate a wide-range solution for crack length of a center cracked specimen, $M(T)$, as a function of compliance, displacement measurement location, and Poisson's ratio. A schematic showing the geometric parameters of an $M(T)$ specimen is given in Figure 1. The total crack length is $2a$ and the nominal distance between the locations for the displacement measurement is $2y$. W is the width of the specimen, B is the specimen thickness, and E is Young's modulus. The compliance, C , is the inverse of the slope of the linear portion of the load versus displacement curve.

The relationship of crack length in terms of the previous defined variables is given by,

$$\frac{2a}{W} = A_1X + A_2X^2 + A_3X^3 + A_4X^4 + A_5X^5 + A_6X^6, \quad (1)$$

where $A_1 = 1.22350,$
 $A_2 = -0.699032,$
 $A_3 = 3.25584,$
 $A_4 = -6.65042,$
 $A_5 = 5.54001,$
 $A_6 = -1.66989,$

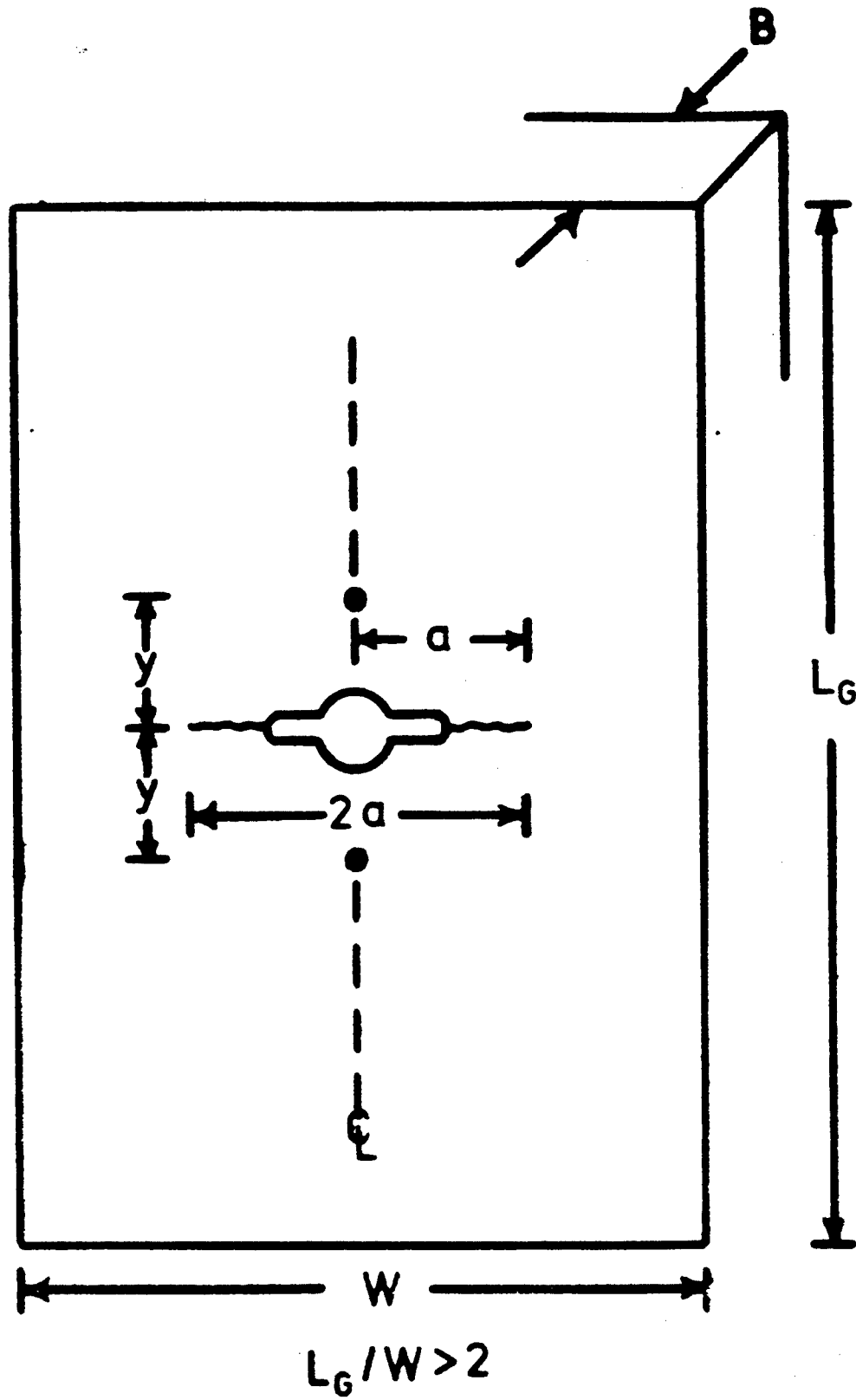


Figure 1. Center-Cracked Tension Specimen-M(T).

and

$$X = 1 - \exp\left[-\frac{\sqrt{(EBC + 2y/W)(EBC - 2y/W)}}{2.141}\right].$$

A comparison of the results of the polynomial expression in equation (1) to available analytical results suggest that the validity of ranges of this expression are $0 < 2a/W < 1$ and $0 < 2y/W < 0.8$ for Poisson's ratio, $\nu = 0.3$.

To account for Poisson's ratio, the A coefficients in equation (1) are replaced with A_i' values, $i = 1, \dots, 6$, where

$$\begin{aligned} A_1' &= A_1 \sqrt{\frac{3.3}{3+\nu}}, \\ A_2' &= A_2 + A_1 \left[1 - \sqrt{\frac{3.3}{3+\nu}}\right], \\ A_3' &= A_3, \quad A_4' = A_4, \\ A_5' &= A_5, \\ A_6' &= A_6. \end{aligned}$$

The details of the development of this equation is described in Reference 1.

2.2 TEST SYSTEM AUTOMATION

Improvements and modifications were made to various test systems to increase their efficiency. A number of test and data reduction software were developed for the IBM 9000 microcomputer to aid different projects in the laboratory. The C20 HCF/LCF system was equipped with an IEEE-488 interface to allow the VIC-20 computer to address two HP multimeters and a Wavetek signal generator to increase the accuracy as well as the

efficiency of the system. Several modifications were also made to the software of the PC test control systems which allowed improved tracking and storage of the load-displacement data.

2.2.1 Software Enhancements on IBM System 9000

Additional test and data reduction software for the IBM System 9000 microcomputer has been developed to aid in some of the test projects in the laboratory. The following packages are now available:

AUTOFCG Version 5.00 and 5.0a - Upgraded versions of the compliance based fatigue crack growth software, including support for HP5316A counter and automatic closure load calculation.

AUTOEP Version 5.00 and 5.0a - Upgraded versions of the automated electric potential crack growth software, including support for HP5316A counter.

AUTOIDG Version 4.22 - Upgraded version of the IDG control program.

SPIDG - A special IDG data reduction program designed to evaluate hysteresis loops taken from C(T) samples near the crack tip.

Produces a closure load and compliance value as well as estimated crack length.

CLLD - A modified version of SPIDG which allows interactive manual selection of the closure load.

A number of other enhancements to various existing programs have been made at the request of the technical and professional staff to suit their specific requirements.

2.2.2 Improvements to the C20 HCF/LCF System

The C20 system has been equipped with an IEEE-488 interface which allows the VIC-20 computer to address two HP multimeters and a Wavetek signal generator. The use of these multimeters provides the accuracy needed for electric potential measurement and simplifies measurement of the minor load signal. The IEEE controlled signal generator provides more accurate and easier to use minor load control than was provided through the previous interface to the old Bruel and Kjaer shaker controller.

2.2.3 Software Enhancements for PC Test Control System

In previous work [2], software was developed to conduct an automated crack growth test under a periodic single-overload fatigue spectrum. A schematic of the applied load and the parameters that describe the load spectrum are shown in Figure 2. Several modifications were made to the software to support several research projects.

The program was modified so that the operator could automatically have hardcopies of the load-displacement data made both before and after each overload. Also, the load-displacement data could be stored on floppy disk or hard disk for subsequent analysis.

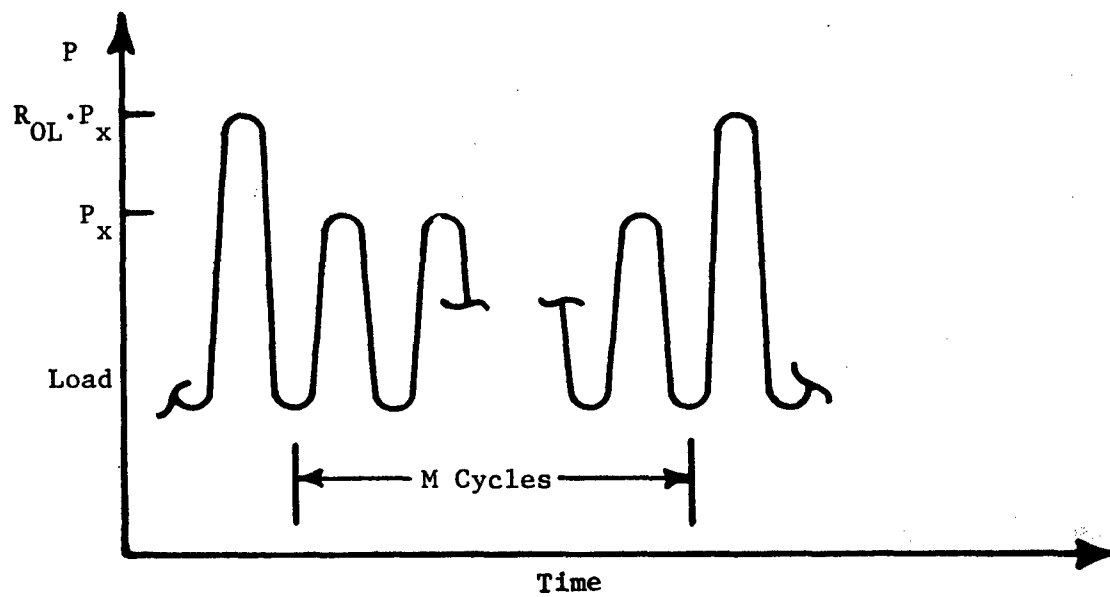


Figure 2. Periodic Single Overload Spectrum.

The original program used compliance information from crack mouth opening displacement measurements to determine crack lengths for C(T) specimens. The capability to use back-face strain compliance for crack length determination was added to the program to support higher test frequency requirements and to facilitate testing at elevated temperatures.

For the software that supports more common fatigue crack growth tests, an option was added to determine crack length from back-face strain measurements on single-edged cracked specimens.

2.3 REPAIR AND IMPROVEMENT OF THE INSTRON MAJOR/MINOR SYSTEM

The Instron system was removed from service due to a burned out armature. This problem and several others associated with the equipment were identified and fixed in the past year.

The armature failure was traced to loose roller guides which allowed the moving armature to contact the fixed structure resulting in damage to the armature winding. The armature has been rewound by Environmental Equipments Ltd. (EEL), an English firm who, in 1984, acquired manufacturing rights for the Instron vibration products.

A number of problems were corrected in the water-cooling circuit (for the shaker and power amplifier). The armature circuit was also noted to be partially clogged with debris and the pressure interlock switches were inoperative because of the debris. Heat exchanger erosion was found

to be the source of the debris, and the original aluminum heat exchanger has now been replaced with one of gun metal construction.

While reinstalling the armature, the water hoses and inoperative temperature switches in the armature were also replaced. Pressure gages were added to the armature inlet and outlet. The pressure switches were replaced with functioning switches.

A water-saver valve was installed on the external side of the heat exchanger - not so much in interest of conserving water - but to prevent over-cooling of the system.

At the recommendation of EEL, a redesigned three-phase protection circuit board was installed in the power amplifier. Also, the output current meter, which was defective, was repaired.

To minimize future shutdown, the following improvements in preventative maintenance have been suggested:

- Periodic inspection of the armature roller guides based on system operational time. This will require partial disassembly of the shaker.
- Close attention to load train alignment.
- Proper grip torquing procedure to eliminate any torque transfer to the armature.

- Monitoring the waterflow in armature cooling circuit by means of the new pressure gages provided.
- Periodic replacement of the distilled water in the cooling-water system.

SECTION 3

MATERIAL CHARACTERIZATION

3.1 CRACK CLOSURE

It is well known that the fatigue crack growth behavior of a material is influenced by crack closure phenomenon. However, a clear understanding of the closure mechanism is not available. In our attempt to improve this understanding, tests were conducted to study the effects of load history and specimen geometry on the fatigue crack closure measurements. In a separate study, the effect of closure on the growth of surface cracks was also investigated by conducting fatigue crack growth experiments on surface flaws introduced in a high-strength titanium alloy.

3.1.1 Effects of Load History and Specimen Geometry on Fatigue Crack Closure Measurements

The phenomenon of crack closure affects the crack growth behavior in materials and hence, any attempt to predict the usable life of components under fatigue loads must account for crack closure. However, values of crack closure presented in the literature have been inconsistent and various closure models seem to predict only limited sets of data. Crack closure is induced by many mechanisms; two important ones in this study are fracture surface roughness and the plastic wake. For these mechanisms, crack closure is dependent upon load history and structural geometry, especially the structural thickness.

The effects on crack closure measurements of simple load histories and specimen sizes were investigated. Tests were conducted on compact type, C(T), specimens having various thicknesses and in-plane dimensions. The simple load histories were composed of constant amplitude load and stress intensity ranges.

Closure load was determined from data collected from three measurement techniques. In the first technique, a clip gage was used to determine the load-displacement behavior at the crack mouth. As a second method, a strain gage was placed on the back-face of the C(T) specimen to determine the load-strain behavior. The third technique employed a laser interferometric displacement system where load-displacement data were collected at various locations on the side of the specimen in the vicinity of the crack tip. Details of this investigation are presented in Reference 3.

3.1.2 Effect of Closure on the Crack Growth of Surface Cracks in a High Strength Titanium Alloy

Fatigue crack growth experiments were conducted on surface flaws in a high strength titanium alloy. Cracks were initiated from semicircular notches introduced by electro-discharge machine (EDM) having approximate dimensions of 100 microns deep by 200 microns wide and having a height of 70 microns. Surface crack lengths in the range of 400 microns to 8 mm were investigated under both increasing and decreasing K conditions. Cracks lengths and closure loads were determined from load-displacement data obtained with the aid of a laser interferometric displacement gage which had a resolution capability of 0.1 micron. Stress

ratios of 0.1, 0.5, and -1.0 were utilized. Crack growth rates were compared for all three stress ratios as a function of ΔK and ΔK_{eff} which was determined from the closure data. The use of effective stress intensity range consolidated most of the data in a small band. The test procedure and results are discussed in Reference 4.

3.2 FATIGUE CRACK GROWTH BEHAVIOR OF IN718

Data were generated under different test conditions to model the fatigue crack growth behavior of IN718 for various load, temperature, specimen geometry and environment. Fatigue crack growth experiments were conducted at 649°C under conditions of high load ratio and frequency to study the interaction of cycle- and time-dependent crack growth. In a separate study, the influence of environment was studied as a function of load ratio and frequency by conducting tests in laboratory air and in an inert environment of a vacuum of 10^{-5} torr. In addition, the fatigue crack growth behavior of a short crack originating from a notch was investigated by conducting tests on C(T) specimens with a keyhole at 650°C and a frequency of 1 Hz.

3.2.1 Fatigue Crack Growth at High Load Ratios in the Time-Dependent Regime

Experimental crack growth rates were determined in Inconel 718 M(T) specimens at 649°C under conditions of high load ratio (R) and frequency (10 to 100 Hz). Under these conditions, the material displays cycle-dependent crack growth as well as time-dependent crack growth. At R values approaching unity, the observed growth rates were lower than those

obtained under sustained load at the same mean load in the absence of the superimposed cyclic loading. Tests on C(T) specimens at lower frequencies were used to demonstrate the existence of three regions of behavior -- cycle-dependent, mixed mode, and time-dependent.

A linear cumulative damage model was used to predict the growth rates due to combined cycle-dependent and time-dependent mechanisms. The model was developed from 427°C data for the cyclic term and sustained load crack growth data obtained at 649°C for the time-dependent term. Although the model could not predict the synergistic effect at high R, it provided a reasonable representation of much of the data. It was concluded that the use of low temperature data for the cyclic term was inadequate for representing the threshold values and growth rates at low ΔK values at the higher temperature. Details of this investigation are presented in Reference 5.

3.2.2 Environmental Interaction as a Function of Frequency for Inconel 718

In previous work [6], crack growth of Inconel 718 has been studied as a function of frequency and stress ratio (R) for a K_{max} value of 40 MPa $\cdot\sqrt{m}$ at 650°C in air environment. Crack growth rate and micromechanisms of growth were found to be a function of frequency for a given R value and could be separated into three distinct frequency regimes - fully time-dependent behavior for lower frequencies, fully cycle-dependent behavior for higher frequencies, and mixed controlling micromechanisms for intermediate frequencies. Increasing values of K were

found to shift the transition frequencies of these behavior regimes towards higher frequency values.

This investigation was extended to study the crack growth rate of Inconel 718 in vacuum [7]. Frequencies ranging from 0.001 to 5 Hz were used to investigate the influence of frequency and environment on crack growth. Three R values (0.1, 0.5, and 0.8) were employed in the study. Observed growth rates and micromechanisms of crack growth in vacuum are being compared with that obtained in air environment. This study was intended to evaluate the influence of oxygen in the environment on the rates and micromechanisms of crack growth.

3.2.3 Crack Growth From Notches

In aircraft engine components, cracks normally initiate from the locations of stress concentrations such as notches and inclusions. Short cracks originating from these stress concentrations initially grow through a decreasing notch-affected stress field. Due to the 'short crack' effect, initial growth rates may not be correlated by the parameters that are typically used to correlate long crack growth rates. When the notch tip stress is higher than the yield strength of the material, the notch is enveloped by a plastic zone. In this case, the cracks which are initiated at the stress concentration locations initially grow through the plastic zone. The early growth of the short crack is within the notched plastic zone. At higher temperatures, the problem of predicting the life of a short crack is further complicated by the time-dependent effects of the material on the notch plastic zone. Due to these

complications, it is very important to understand the behavior of short cracks at the notches to develop improved life prediction models for aircraft engine components operating at elevated temperatures.

An investigation was initiated to study and understand the growth of cracks from a notch. C(T) specimens with a keyhole were fabricated for this study. The tests were conducted at 650°C on Inconel 718 specimens at a frequency of 1 Hz. The entire specimen, including the notch, was first mechanically polished. Then the specimen was electro-polished to remove any residual stresses created by the mechanical polishing process.

During the tests, crack lengths were monitored both with electric potential and compliance methods. The electric potential technique was found to be more precise for detecting the crack initiation as compared to compliance method.

The crack growth tests were conducted at two different load levels of 1,150 lbs. and 574 lbs. These loads were chosen to create two conditions - a notched plastic zone produced by higher load and an unaffected one (negligible plastic zone) by the lower load. Since a crack could not be initiated at 574 lbs. in the first few tests, the load was increased to 750 lbs. According to calculations, a very small zone of plasticity at 750 lbs. is created at the notch but the size of this plastic zone is expected to be smaller than the length of the smallest crack that could be measured. In this case, the crack growth rates were measured outside the plastic zone of the notch and cracks were grown until

the crack length was 0.15 inch from the notch tip of the specimen. Figure 3 shows the crack growth rates as a function of crack length for the two loads tested. At the smaller load of 750 lbs., fatigue crack growth rate increases continuously with the crack length. In the test which was conducted at the higher load of 1,150 lbs., the crack growth rate initially decreases and then increases with the increasing crack length. This anomaly in crack growth rate is apparently caused by the interaction of the notch plastic zone with the crack growth process. As the stress intensity monotonically increases from a value of zero at the notch tip with the increasing crack length, K cannot be used to fully correlate the crack growth rate at the vicinity of the notch.

More tests will be conducted utilizing triangular waveforms with lower frequencies and hold-times to evaluate the time-dependent effect on the crack growth rate for cracks initiating from the notch at the higher load level.

3.3 CRACK GROWTH BEHAVIOR OF SINGLE CRYSTALLINE MATERIAL

Fatigue and creep crack growth behavior of an advanced nickel-base superalloy single crystal were investigated over a wide range of temperatures. The influence of environment on the fatigue and creep crack growth characteristics was studied by conducting tests in laboratory air and a vacuum of 10^{-5} torr. Tests were also conducted with crystal tensile axis and crack growth direction aligned in several orientations to investigate the influence of anisotropy on elevated temperature crack

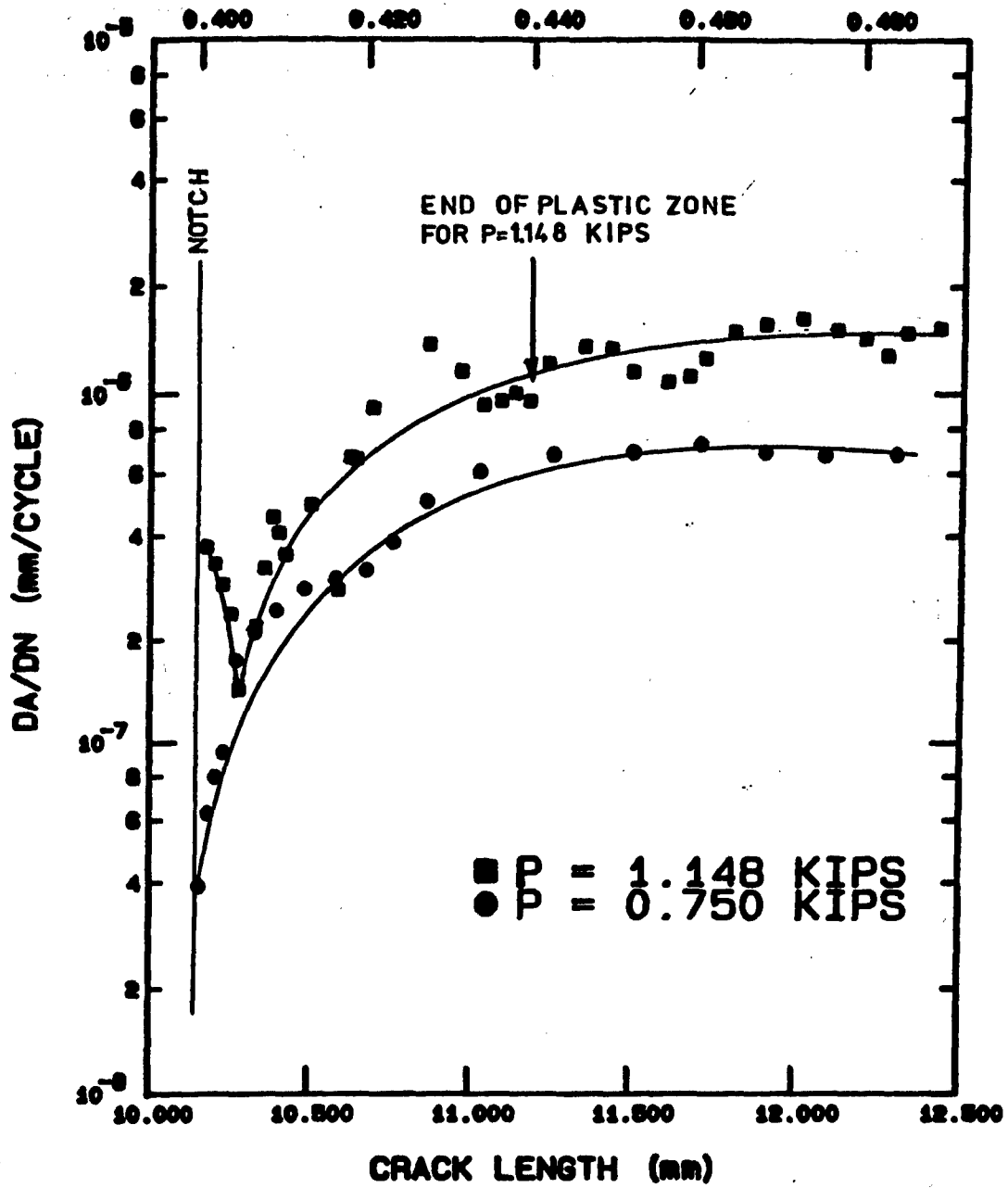


Figure 3. da/dN vs. Crack Length Behavior of Crack Growing From a Notch.

growth behavior. Detailed fractographic analysis were conducted to understand the prevailing mechanism under specific conditions.

3.3.1 Fatigue Crack Growth in Alloy N4

The effect of crystal anisotropy on the fatigue crack growth has been investigated by conducting constant load fatigue crack growth tests with two crystal orientations of $\langle 101 \rangle / \langle 010 \rangle$ and $\langle 010 \rangle / \langle 001 \rangle$ tensile/crack orientations (the tensile loading axes are parallel to $\langle 101 \rangle$ and $\langle 010 \rangle$ and crack growth directions are parallel to $\langle 010 \rangle$ and $\langle 001 \rangle$, respectively). All the tests were conducted over the temperature range of 1200 to 1600°F. The testing over this wide range of temperature provided information on the influence of temperature on fatigue crack growth. Detailed fractographic analysis of the failed specimens were conducted to determine the crack growth mechanism. Reference 8 presents the details of this study.

3.3.2 Fatigue Crack Growth of Alloy N4 in Vacuum

Fatigue crack growth tests in vacuum of nearly 10^{-5} torr were conducted under similar temperature and load conditions utilized for tests conducted in air. Tests conducted at 1600°F indicated a higher crack growth rate in vacuum as compared to laboratory air. This anomaly in behavior is being further investigated. Threshold tests were also conducted where the influence of environment is expected to be most pronounced. Details of this study are presented in Reference 8.

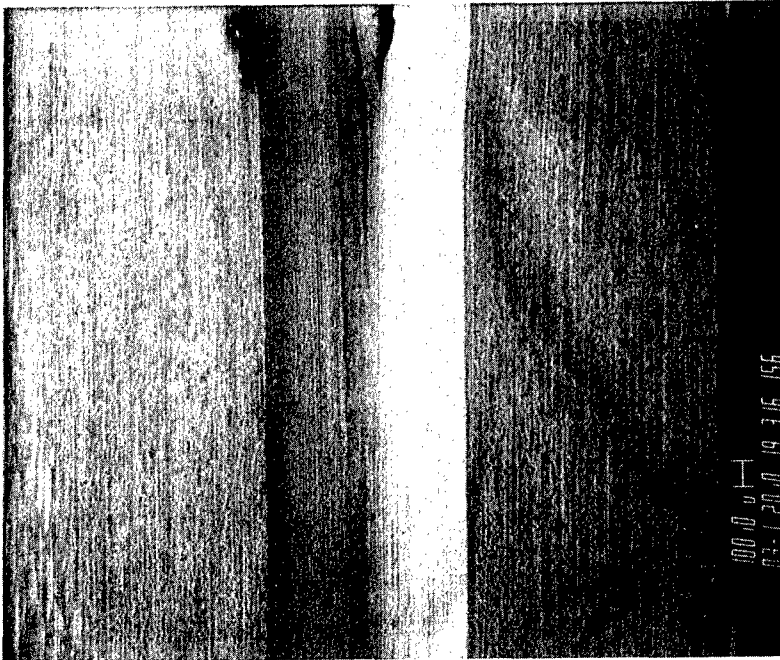
3.3.3 Creep Crack Growth of Alloy N4 in Laboratory Air

The effect of temperature on the creep crack growth (CCG) behavior of advanced nickel-base superalloy Rene' N4 single crystals was studied earlier [8] by conducting tests in the temperature range of 1600°F to 1900°F. All the specimens used in this investigation were oriented in $\langle 001 \rangle / \langle 010 \rangle$ tensile/crack orientation.

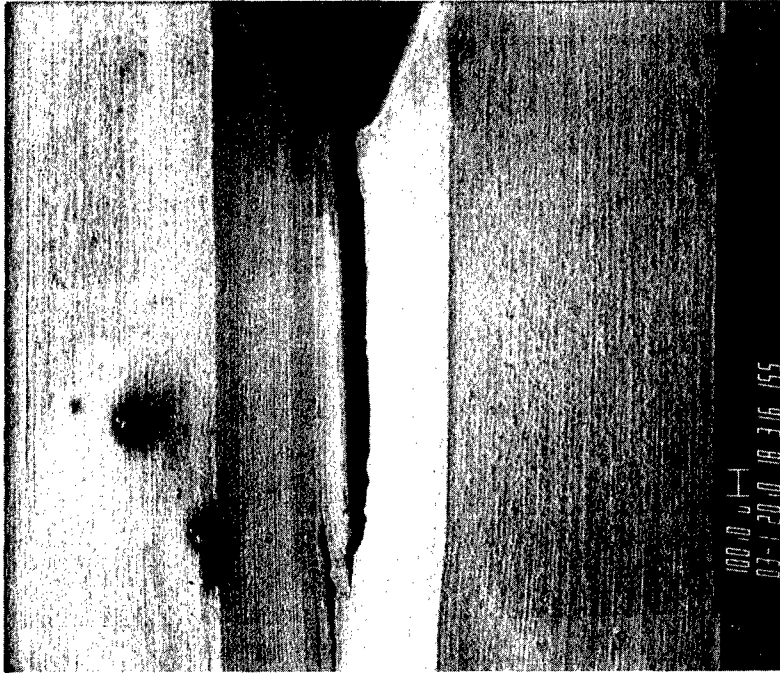
Currently, the effect of anisotropy is being studied in detail with specimens having $\langle 010 \rangle / \langle 101 \rangle$ orientation. Specimens have also been fabricated with $\langle 101 \rangle / \langle 010 \rangle$ orientations, tests are planned for next year. Two tests were conducted with side-grooved subcompact tension specimens with $\langle 101 \rangle / \langle 010 \rangle$ orientation at 1600°F in laboratory air. In both tests, a phenomenon of crack layering as shown in Figure 4 was observed after an initial growth of 50 to 100 mm, resulting in crack arrest. Figure 4(a) shows the extension of crack layering far ahead the crack tip. Figure 4(b) shows the overall crack along with layered cracks. The reason for such crack layering is being investigated. Previously, layering has also been observed with side-grooved subcompact IN718 specimens tested at 1000°F under static load.

3.3.4 Creep Crack Growth of Alloy N4 in Vacuum

CCG tests in vacuum are being conducted to provide baseline results for evaluating the influence of environment on CCG behavior of alloy N4 single crystals. The vacuum tests are being conducted on subcompact tension specimens precracked to an unusually high precrack



a. Low Magnification Picture Showing Crack Layering Ahead of Crack Tip.



b. Higher Magnification of Crack.

Figure 4. Crack Layering.

length of 0.44 inches ($a/W = 0.52$) to obtain a relatively high initial stress intensity value that is within the load capacity of the loading pins and grips. The results of the test conducted on specimens with $\langle 101 \rangle / \langle 010 \rangle$ orientation in vacuum at 1600°F is shown in Figure 5. The CCG behavior appears to be similar to that of specimens with $\langle 001 \rangle / \langle 010 \rangle$ orientation as shown in Figure 6. However, the crack front was nearly 34° off from $\langle 010 \rangle$.

It was noted that in all orientations studied, the crack front is parallel to primary dendrite. However, results compared with a test conducted with $\langle 001 \rangle / \langle 010 \rangle$ specimen with crack front only 3° away from $\langle 010 \rangle$ shows similar growth rates. The general observation is that creep crack growth is rapid at relatively high stress intensities of 45 to $55 \text{ MPa} \cdot \sqrt{\text{m}}$. At levels of stress intensity in the range of 35 to $45 \text{ MPa} \cdot \sqrt{\text{m}}$, no growth has been observed over 100 hours.

3.3.5 Fracture Surface Analysis of Creep Crack Growth Specimens

The fracture surface of the specimens tested in air and vacuum were observed under SEM to determine the failure mechanisms. The results are discussed in Reference 8.

3.3.6 Creep Crack Growth of IN718

Several tests were conducted with SEN specimens that were 0.4-inch thick, twice as thick as the 0.2-inch thick mini-compact specimens. Tests were conducted both in air and vacuum at 1200°F to

86-281 1600F HI-VAC

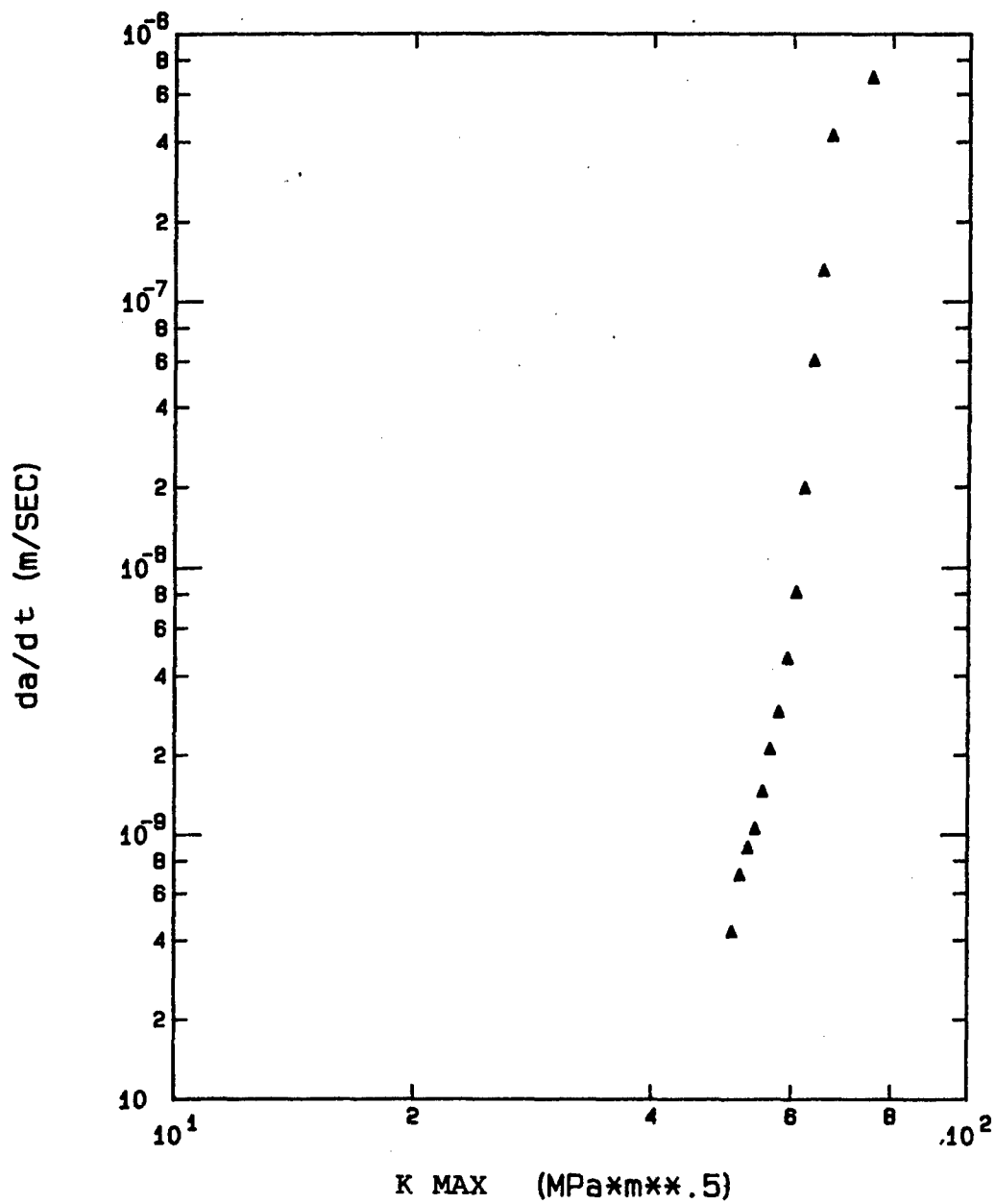


Figure 5. Crack Growth Behavior of Specimen with $\langle 101 \rangle / \langle 010 \rangle$ Orientation Tested at 1600°F in Vacuum.

evaluate the influence of specimen thickness. The test results from the thicker SEN specimens are shown in Figure 7. The CCG behavior is very similar to that obtained earlier [9] with 0.20-inch thick specimens. Apparently, the effect of specimen thickness is negligible over this range of specimen thickness.

3.4 MICROSTRUCTURE EVALUATIONS OF CREEP RUPTURE IN SINGLE CRYSTALLINE MATERIAL

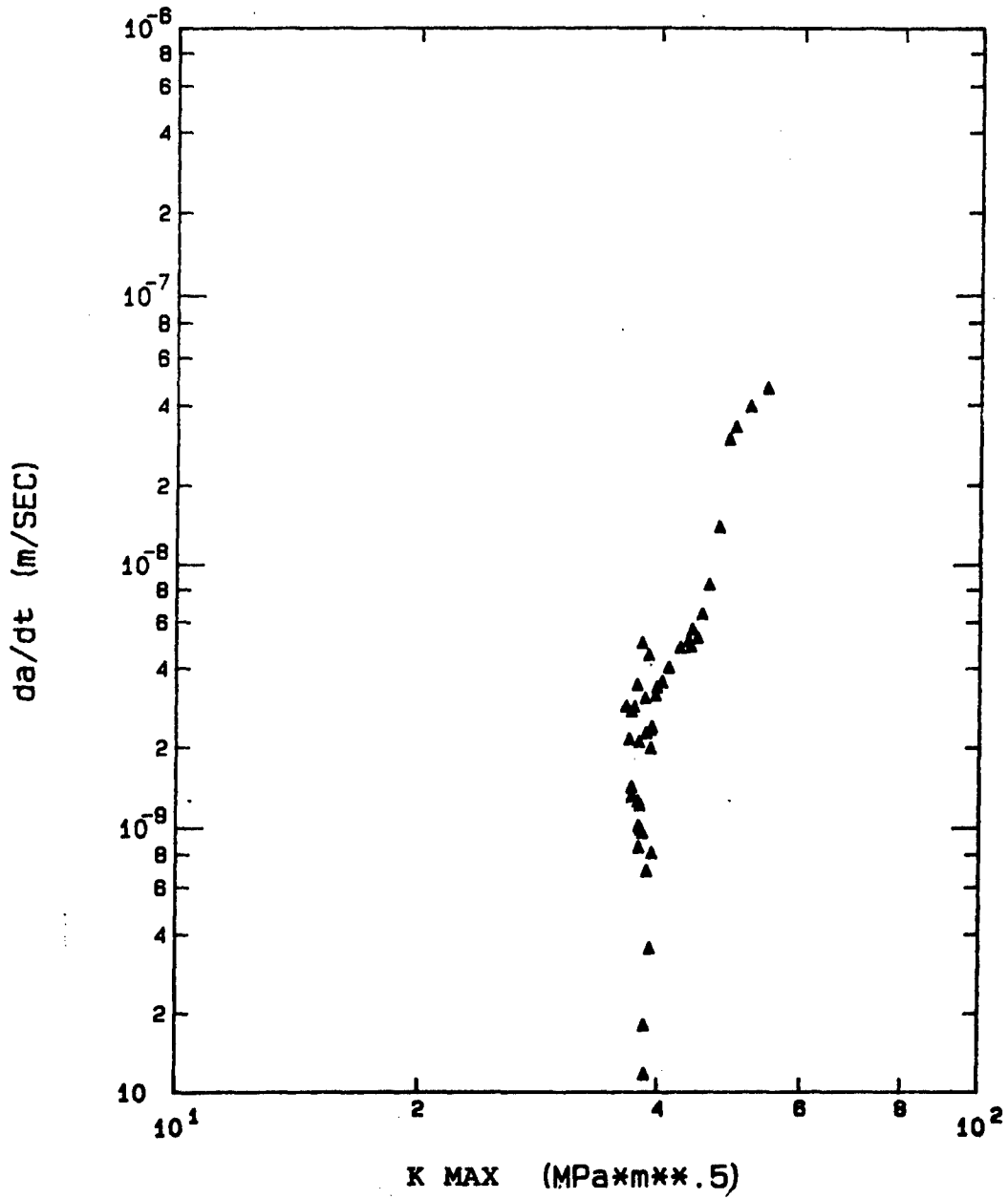
A detailed microstructural evaluation of the creep processes occurring in a single crystalline material over the temperature range of 1400°F to 2000°F was carried out through transmission electron microscopic analysis. The various stages of deformation process and the substructure developed in the primary, steady, tertiary, and rupture regimes were investigated by analyzing the microstructure developed at different amounts of creep strain. Details are covered in the following section.

3.4.1 Creep Rupture Tests of Alloy N4

Creep rupture tests of single crystals of gamma prime precipitation hardened Rene' N4 with the tensile axis parallel to $\langle 001 \rangle$, over the temperature range of 1400°F to 2000°F have been reported earlier [10].

A detailed TEM analysis of these specimens has been conducted to investigate the progressive development of substructure with increasing creep strain. A number of sustained load creep tests were conducted at 1600°F where the tests were stopped at selected levels of

84-231 SEN 1200F VAC



creep strain in the primary, secondary, and tertiary regions to study the development of substructure at different stages of creep. The results of the TEM analysis are discussed in the following section.

3.4.2 Substructural Analysis of Creep Tested Specimen at 1600°F

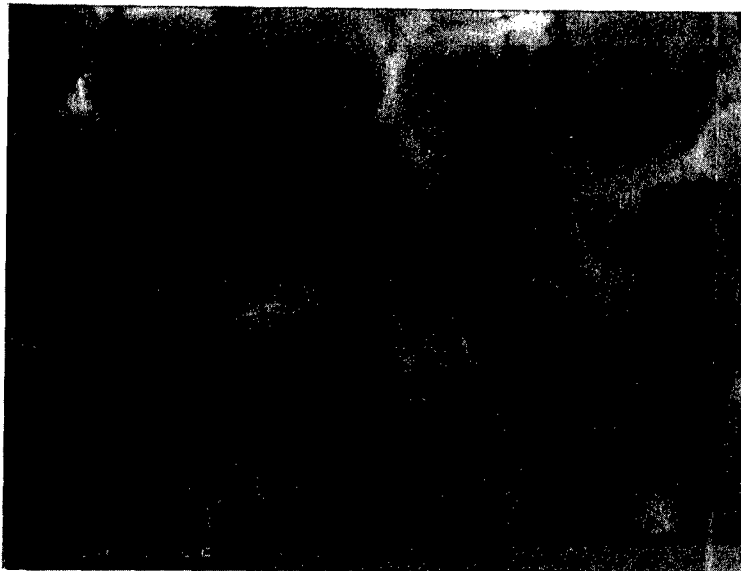
Thin foils were prepared from creep specimens tested in air at 1600 °F to different levels of strain. For comparison, one foil was prepared from the same batch of material to look at the substructure of undeformed heat-treated material. The TEM micrograph shown in Figure 8 represents the general microstructure of heat-treated Rene' N4 alloy. Apparently, the undeformed substructure is free of any dislocations.

Figure 9(a) shows the general feature of the substructure developed at 0.15 percent strain (in the primary creep strain regions) at 1600°F. The presence of dislocations in the matrix and at the interface is noticed. Figure 9(b) provides a higher magnification of another representative area showing again that the dislocations are mainly in the matrix surrounding the precipitate, indicating that their movement has been restricted by gamma prime precipitate.

At a strain of 0.86 percent, which lies in the initial stage of steady-state creep, the development of faults in the precipitate is noticed, as shown in Figure 10(a). At the same time, with increased strain, dislocation interaction leads to the formation of a dislocation network at the interface, as shown in Figure 10(b). Some of the dislocations can be seen entering the precipitate, as shown in Figure



Figure 8. TEM Microstructure of Heat-Treated, Rene' N4 Single Crystal.



a. Tested at 1600°F.



b. Notice the Dislocation Surrounding
Gamma Prime Precipitate.

Figure 9. Substructure Developed at 0.15% Creep Strain.



a. Stacking Faults with Precipitate.



b. Dislocation Network at the Interface.

Figure 10. Substructure Developed at 0.86% Creep Strain Tested at 1600°F.

10(c), thus indicating dislocation movement in both the matrix and precipitate.

The dislocation activity intensifies with increased deformation and the general substructural feature of a specimen strained up to 2.5 percent is shown in Figure 11(a). The increase in stacking faults as well as dislocation density is clearly noticed. Figure 11(b) provides another TEM micrograph from the same specimen showing a super pair entangled with stacking faults. The shear or cutting of the gamma prime precipitate by a super dislocation is shown in Figure 11(c). These dislocations were analyzed through the $\bar{g} \cdot \bar{b} = 0$ criterion (where \bar{g} is the reflecting plane vector and \bar{b} is the dislocation Burger's vector), and found to be $a/2 \langle 110 \rangle$ type.

Figure 12 shows the substructure developed at very high strain levels of >10 percent, leading to failure. The substructure is very complex; one notices at least two sets of faults, along with the indication of precipitate shearing by $a/2 \langle 110 \rangle$ super dislocation. Also, there is an intensive network of interfacial dislocation. Although not shown in the micrograph, the development of microtwins was also observed. The complex dislocation structure is indicative of two modes of precipitate shear: one involving the creation of low energy superlattice extrinsic and intrinsic stacking faults by the viscous glide of $a/3 \langle 112 \rangle$ partial dislocations through gamma prime, and the second involving the cutting of gamma prime particles by constricted $a/2 \langle 110 \rangle$ dislocation pairs.

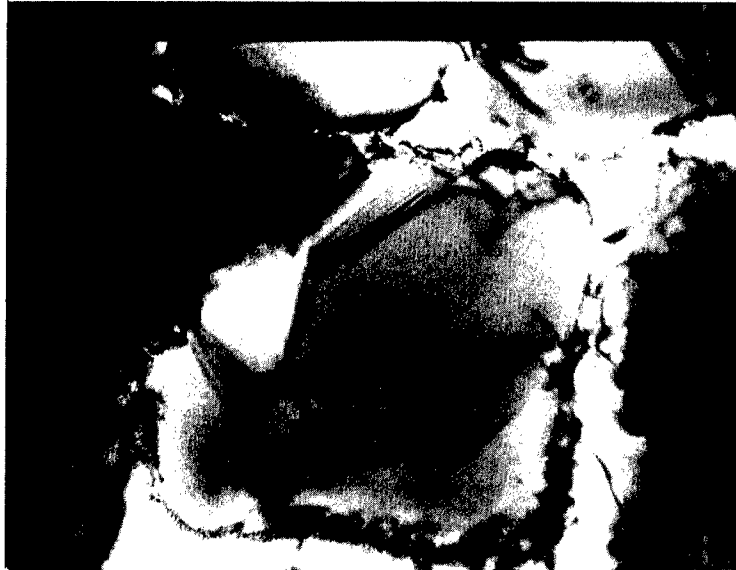


c. Dislocation Migration into Precipitate.

Figure 10 (Concluded).



a. High Density of Stack Fault.



b. Super Pair Entangled with Stacking Fault.

Figure 11. Substructure Developed at 2.5% Creep Strain Tested at 1600°F.



c. Precipitate Shear by Super Pair.

Figure 11 (Concluded).

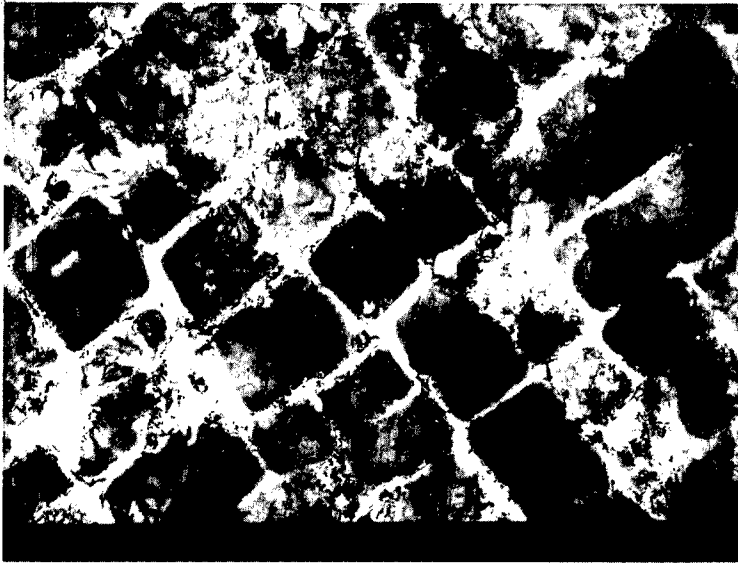


Figure 12. Substructure Developed at $>10.0\%$ Creep Strain
Tested at 1600°F .

3.4.3 Development of Substructure at 1400°F, 1600°F, 1800°F, and 2000°F

Thin foils were prepared from specimens that experienced creep rupture at 1400°F, 1600°F, 1800°F, and 2000°F under sustained loadings of 100 ksi, 65 ksi, 30 ksi, and 12.5 ksi, respectively, to investigate the difference in creep morphology with temperature. Figure 13(a) is a low magnification (20,000X) TEM micrograph showing heavily faulted structure of the specimen failed at 1400°F. Most of the dislocation activity is confined to the precipitate, and the precipitate shear appears to occur by the glide of $a/3 \langle 112 \rangle$ partial dislocations. The faulted structure can be seen more clearly in Figure 13(b), where two sets of faults can be easily distinguished. Similar faulted substructure is observed in the foil prepared from specimens failed at 1600°F. At 1600°F, two sets of microtwins were also observed. One such set of microtwins is shown in Figure 14(a). Although as clear, the microtwin activity on the other set of planes is shown in Figure 14(b). There are some indications that the intersection of such microtwins act as a crack nucleation site. This phenomenon has been observed only at 1600°F and it is postulated that the microtwins are formed by a cooperative stacking of faults.

The substructure is somewhat different for specimens tested at 1800°F. The formation of cells in these substructures is quite evident as shown in Figure 15(a), and hardly any fault is noticed. The cell walls are made up of networks of super pairs of $a/2 \langle 110 \rangle$ dislocations as shown in Figure 15(b). Such dislocation pairs can be seen within the precipitate also, as discussed earlier. In contrast to the deformation

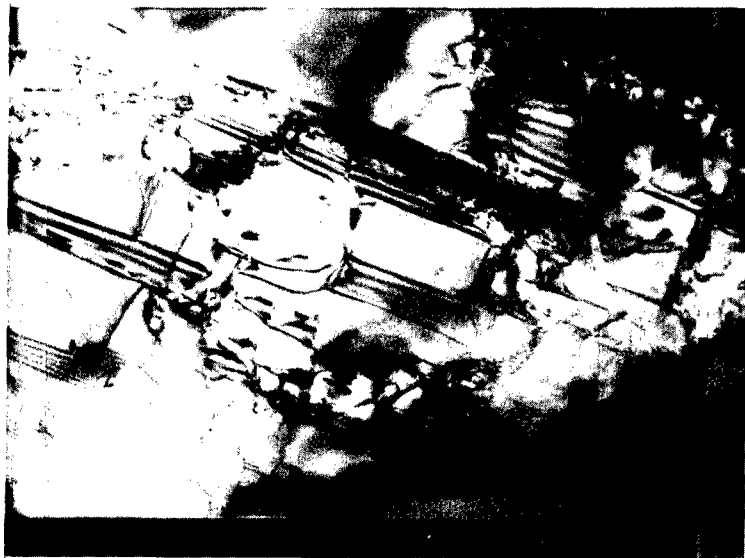


a. High Density of Faults.



b. Two Sets of Faults in the Precipitate.

Figure 13. Substructure Developed in the Creep Ruptured Specimen at 1400°F.



a. Indication of Microtwin Formation from Stacking Faults.



b. Two Sets of Intersecting Microtwins.

Figure 14. Substructure Developed in Creep-Ruptured Specimen at 1600°F.



a. Cell Structure.



b. Network of Super Pair Dislocation.

Figure 15. Substructure Developed in Creep-Ruptured Specimen at 1800°F.

mode at 1400°F, where the deformation was controlled by viscous glide of $a/3 \langle 112 \rangle$ partial dislocation, at 1800°F the deformation mode is predominantly controlled by the glide of super $a/2 \langle 110 \rangle$ dislocation pairs, see Figure 15(c). At the intermediate temperature of 1600°F, both the modes of shear are operative.

The higher temperature of 2000°F leads to the instability of precipitate structure itself and formation of creep cell structures even within the precipitate is observed, as shown in Figure 16(a). The deformation cell is more clearly shown in Figure 16(b), while Figure 16(c) shows the development of cell walls within a precipitate. The cell wall here is composed of $a/2 \langle 110 \rangle$ super dislocation pairs. Figure 16(d) is a higher magnification micrograph of such a cell wall showing the interaction of super $a/2 \langle 110 \rangle$ dislocation pairs.

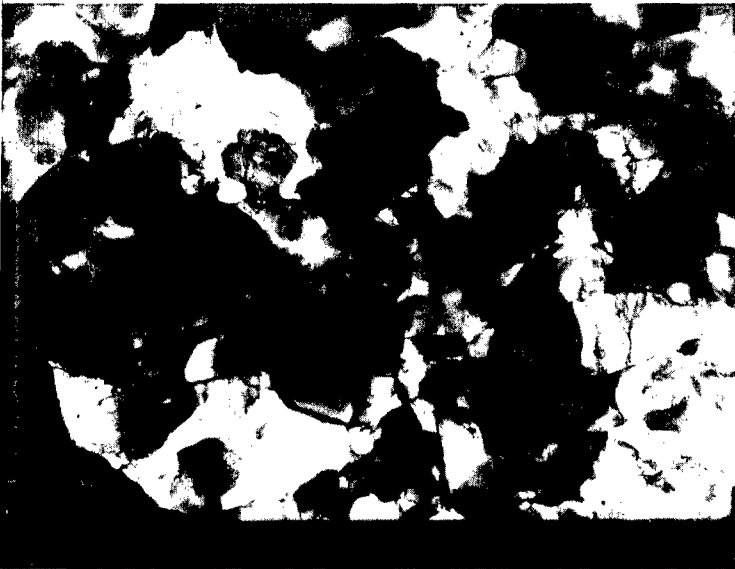
3.4.4 Analysis of Stacking Faults

From earlier observations, it appears that at temperatures higher than 1800°F, where the stacking fault energy of this alloy is quite high, the role of stacking faults in the creep deformation is negligible. At 2000°F, no stacking faults were, in fact, observed. However, for temperatures of 1400°F and 1600°F, the stacking faults play a dominant role in the deformation process. The contribution of these stacking faults to the creep process is of special interest at 1600°F, where the formation of microtwins is believed to be the results of particular arrangements of these stacking faults. Apparently, the intersection of these microtwins serve as nucleation sites for crack initiation.



c. Super Pair Dislocation in Precipitate.

Figure 15 (Concluded).

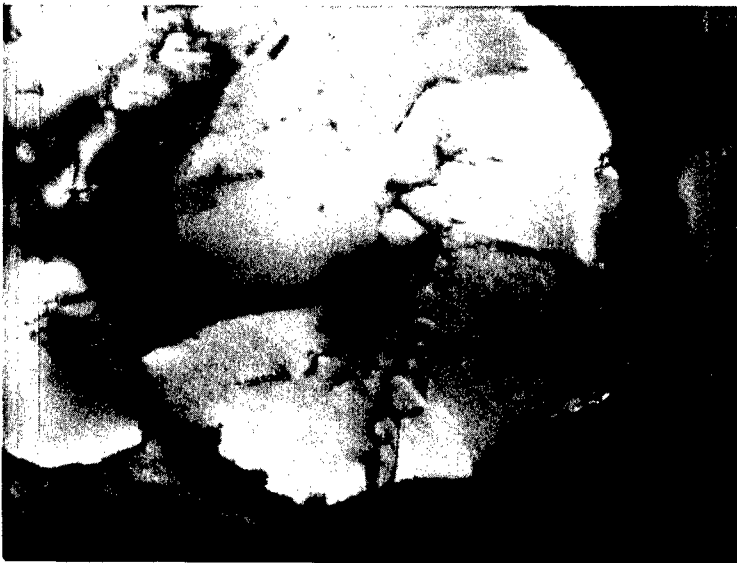


a. Cell Structure.



b. High Magnification of Cell Structure.

Figure 16. Substructure Developed in Creep-Ruptured Specimen at 2000°F.



c. Cell Development Within
Precipitate.

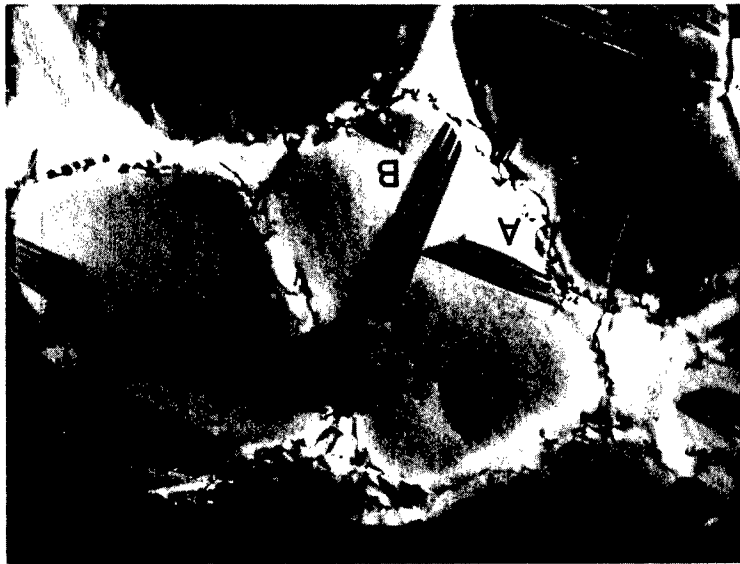


d. $a/2 \langle 110 \rangle$ Super Pair in Cell
Wall.

Figure 16 (Concluded).

A simple analysis of the stacking faults observed at 1600°F was conducted using the $\bar{g} \cdot \bar{R} = 0, 1, \text{ etc.}$, criterion (where \bar{g} is the reciprocal vector and \bar{R} is the displacement vector) to understand the glide mechanism operating. Figure 17(a) shows different sets of stacking faults obtained from a specimen creep ruptured at 1600°F and 65 ksi. The dark field image of these faults is shown in Figure 17(b). For some of these faults, e.g., A and B, the extreme fringes differ in sense; one is bright and the other is dark, indicating that the dislocation form intrinsic/extrinsic faults. Again for a particular reflection of $\bar{g} = 200$, all the stacking faults (A to E) are visible as shown in Figure 17(a). The stacking faults A, C, and E, are, however, invisible for $\bar{g} = \bar{2}20$, as shown in Figure 17(c), indicating the fault plane to be $(11\bar{1})$. These stacking faults were found to be invisible for $\bar{g} = 220$ also.

The faults B and D are invisible for $\bar{g} = 2\bar{2}0$ as shown in Figure 17(d), indicating that these faults lie on $(1\bar{1}1)$ plane. Furthermore, the faults A and B both are invisible for $\bar{g} = 311$, as shown in Figure 17(e). Confirming the fault planes of A and B to be $(11\bar{1})$ and $(1\bar{1}1)$ - this analysis indicates that the deformation process involving the creation of stacking faults is occurring at least on two different sets of (111) plane.

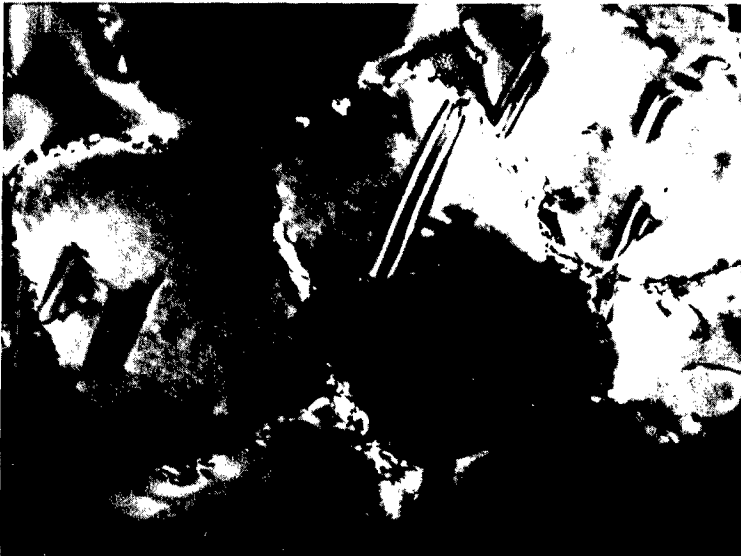


a. Bright Field Image.



b. Dark Field Image.

Figure 17. Different Sets of Stacking Faults Developed at 1600°F.

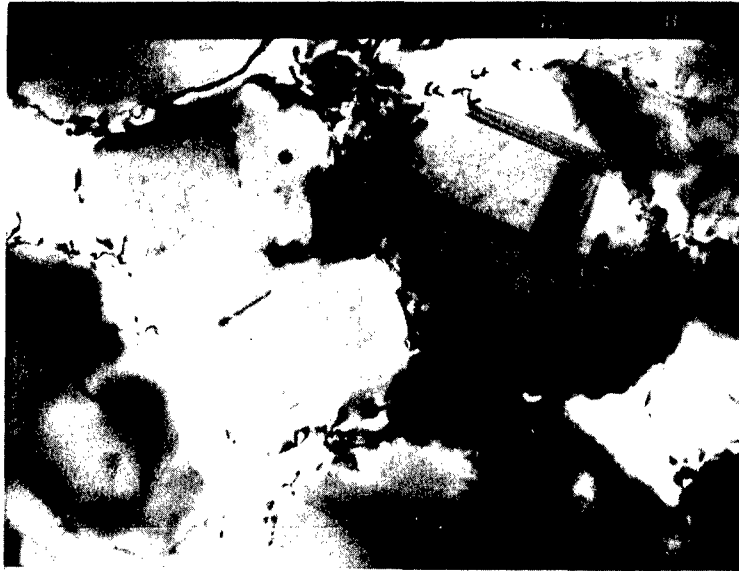


c. Faults A, C, and E Invisible
for $\bar{g} = 220$.



d. Faults B and D Invisible for
 $\bar{g} = 2\bar{2}0$.

Figure 17 (Continued).



e. Faults A and B are Invisible for $\bar{g} = 311$.

Figure 17 (Concluded).

3.5 FATIGUE LOADING AT HIGH FREQUENCY

3.5.1 High Frequency Fatigue Evaluation of Nickel-Base Sheet Material

The objective of the test program was to evaluate the fatigue resistance of a gas turbine burner liner material, HASTELLOY X, under a combination of high frequency fatigue and dwell-cycle fatigue loadings. The high frequency loading test was conducted at 1120 Hz. The period of the combined loading cycle was 20s. The material was tested at 800°F in laboratory air.

All tests were load controlled under tension-tension axial loads and were conducted in resistance heated furnaces. All stresses were calculated using the initial cross-sectional test area of the specimen. No load adjustments were made for changes in test area due to inelastic deformation that occurred during the test. In counting cycles-to-failure, a single cycle was a combined HCF/LCF duty cycle with a 20s period. A specimen that did not fail after 10,000 duty cycles was considered a run-out. Details of this investigation are presented in Reference 11.

3.6 HOT CORROSION TESTS

A study was initiated to study the effect of hot corrosion on creep rupture life of alloy Rene' 77 and Rene' 80. Specifically, the objective was to investigate the effect of stress in the hot corrosion process, and the microstructural changes and mechanisms which occur during corrosion-mechanical property interactions. Sustained load creep tests using

smooth, round bar specimens were conducted at temperatures of 800°C and 1000°C at stress levels ranging from 15 ksi to 75 ksi. Specimens were coated with a thin film of 90% Na₂SO₄/10% NaCl solution to obtain the hot corrosion environment at elevated temperature. Tests conducted with salt coated specimens were compared with tests conducted with uncoated specimens. A successful attempt has been made to correlate stress level, temperature, and environmental damage as measured by depth of penetration to examine the effect of stress on environmental attack. Details of this study are available in Reference 12.

SECTION 4

DATA MAINTENANCE AND TEST SUPPORT ACTIVITIES

As an essential part of our research activity, we have developed a procedure in which all the data generated in the laboratory is transmitted to a central HOST computer for manipulation and storage. This system was continuously maintained and updated. In this program, various types of mechanical tests were also conducted to support the material characterization research activities of other branches.

4.1 DATA TRANSMISSION AND STORAGE

The data generated in the laboratory is transmitted to the central laboratory HOST computer for manipulation and storage. The transmission can be made via a number of serial RS232 communication ports attached to various microcomputers at the test stations. A set of data manipulation, reduction, and plotting routines are maintained on the HOST computer (PDP 11/24) for general use. In addition, cartridge tape and removable hard disk media archival facilities are available for all users. All critical data and software, including the system software, are backed up on both tape and disk.

4.2 MLLS BRANCH TEST SUPPORT ACTIVITIES

Various tests are conducted in the laboratory to provide basic mechanical property data on existing and developmental materials. The

procedures set forth in the ASTM Standard Test Methods are followed for these tests unless otherwise specified by the engineer/scientist.

The types of tests that have been performed during the past year are fatigue crack growth at room temperature, axial fatigue at room temperature, fracture toughness at room temperature, and tensile tests from room temperature to 316°C. These tests were performed on numerous alloys of aluminum and titanium. After each test, the data were analyzed, documented, and reported to the respective project engineer.

SECTION 5

SUMMARY

This report describes a one-year effort on a multi-task research and development activity being conducted to establish a sound life prediction methodology for elevated temperature materials including composites. During the period, substantial effort was devoted to the characterization of crack growth behavior of nickel-base superalloys. Various experiments dealing with crack closure, fatigue crack growth behavior, HCF/LCF behavior, creep/fatigue interaction, and environmental effects on creep/fatigue characteristics were conducted using the automated test facilities in our laboratory.

During the past year, the capability of the IDG laser system to monitor the gage length over 0.1 mm to approximately 10 mm was evaluated and found feasible. In the area of composite testing, a new flat plate friction grip with proper specimen geometry was designed and fabricated. A number of tests and data reduction software was developed for the IBM 9000 microcomputer to improve our test automation system. The C20 HCF/LCF system was equipped with an IEEE-488 interface and several modifications were made to the software of PC control systems to increase the efficiency of existing measurement techniques.

The effects of load history and specimen geometry on the fatigue crack closure was studied to better understand the closure phenomenon. In this context, the effect of closure on the fatigue of surface crack growth of a high-strength titanium alloy was also investigated. Major effort was

devoted to further investigate the fatigue crack growth behavior of IN718 under various load, temperature, and environmental conditions. The role of specimen geometry was included in this investigation. This work was extended to investigate the fatigue crack growth behavior of short cracks starting from notches. IN718 was chosen as a model material and most tests were conducted at 649°C.

In our effort to characterize an advanced material, the fatigue and creep crack growth of a nickel-base single crystal alloy N4 was studied over a wide temperature range of 1400°F to 2000°F. The effect of frequency, environment, and anisotropy on crack growth behavior was also investigated. In addition, the microstructural evaluation of the substructure developed at different stages of creep was carried out through TEM analysis to understand the mechanism of creep deformation in single crystalline material. TEM specimens were obtained from creep rupture tests conducted over the wide temperature range of 1400F to 2000°F which were stopped at predetermined amounts of creep strain.

In this program, the effect of a more realistic and aggressive environment on the elevated temperature mechanical behavior of nickel-base superalloy was also studied by investigating the stress assisted hot salt corrosion of Rene' 77 and Rene' 80 alloy.

Other activities included the support for mechanical characterization of materials for the MLLS Branch. In support of the experimental investigation, the data generated in the laboratory was

transmitted to the central laboratory HOST computer for manipulation and storage, and the system is continuously maintained for all users.

REFERENCES

1. Ashbaugh, N. E., "Crack Length Expression as a Function of Compliance for Center-Crack Tension Specimen," ASTM Research Report RR-E24-1012, June 1986.
2. Ashbaugh, N. E., Khobaib, M., Hartman, G. A., Weerasooriya, T., Rajendran, A. M., Maxwell, D. C., and Goodman, R. C., "Research on Mechanical Properties for Engine Life Prediction," AFWAL-TR-85-4154, Wright Aeronautical Laboratories, Air Force Materials Laboratory, Wright-Patterson Air Force Base, Ohio, May 1986.
3. Ashbaugh, N. E., "Effect of Load History and Specimen Geometry on Fatigue Crack Closure Measurements," Submitted for Review to ASTM STP of International Symposium on Fatigue Crack Closure, August 1986.
4. Jira, J. R., Weerasooriya, T., Nicholas, T., and Larsen, J. M., "Effects of Closure on the Fatigue Crack Growth of Small Surface Cracks in a High Strength Titanium Alloy," Presented at the International Conference on Closure, South Carolina, May 1986.
5. Nicholas, T. and Ashbaugh, N. E., "Fatigue Crack Growth at High Load Ratios in the Time-Dependent Regime," Submitted for Review to ASTM STP of Proceedings of the 19th National Symposium on Fracture Mechanics, September 1986.

6. Weerasooriya, T., "Effect of Frequency on Fatigue Crack Growth Rate at High Temperature," Presentation Given at Sixteenth National Symposium on Fracture Mechanics, Columbus, Ohio, August 1983.
7. Weerasooriya, T. and Nicholas, T., "Application of Crack Growth Maps to Elevated Temperature Fatigue," Presentation Given at the TMS/AIME Fall Meeting, Orlando, Florida, October 1986.
8. Venkataraman, S., Nicholas, T., and Khobaib, M., "Creep and Fatigue Crack Growth Behavior of Single Crystal Rene' N4 Advanced Nickel-Base Superalloy," Presented at TMS/AIME Fall Meeting, Orlando, Florida, October 1986.
9. Stucke, M., Khobaib, M., Mazumdar, B., and Nicholas, T., "Environmental Aspects in Creep Crack Growth in a Ni-Base Superalloy," Proceedings of the Sixth International Conference on Fracture, New Delhi, INDIA, 6 December 1984.
10. Khobaib, M. and Nicholas, T., "The Effect of Pack Aluminized Coating on the Creep Behavior of Rene' N4 Advanced Ni-Base Superalloy," Presented at the TMS/AIME Fall Meeting, Toronto, Canada, October 1985.
11. Ashbaugh, N. E. and Goodman, R. C., "A Fatigue Evaluation of Hastelloy X Sheet Material," Technical Report UDR-TR-86-57, University of Dayton Research Institute, Dayton, Ohio, June 1986.

12. Balsone, S. J., Nicholas, T., and Khobaib, M., "The Effect of Stress on the Environmental Attack of Rene' 80," Presented at the TMS/AIME Fall Meeting, Orlando, Florida, October 1986.